The electronic structure of tungsten oxide thin films prepared by pulsed cathodic arc deposition and plasma-assisted pulsed magnetron sputtering

2008 J. Phys.: Condens. Matter 20 175216

(http://iopscience.iop.org/0953-8984/20/17/175216)

J. Phys.: Condens. Matter **20** (2008) 175216 (7pp) doi:10.1088/0953-8984/20/17/175216

The electronic structure of tungsten oxide thin films prepared by pulsed cathodic arc deposition and plasma-assisted pulsed magnetron sputtering

M R Field[1], D G McCulloch[1], S N H Lim[2], A Anders[3], V J Keast[4] and R W Burgess[4]

[1] Applied Physics, School of Applied Sciences, RMIT University, GPO Box 2476V, Melbourne 3001, Australia
[2] School of Physics, University of Sydney, NSW 2006, Australia
[3] Lawrence Berkeley National Laboratory, University of California, 1 Cyclotron Road, Berkeley, CA 94720, USA
[4] School of Mathematical and Physical Sciences, The University of Newcastle, Callaghan, NSW 2308, Australia

E-mail: matthew.field@student.rmit.edu.au

Received 20 December 2007, in final form 6 March 2008
Published 7 April 2008
Online at stacks.iop.org/JPhysCM/20/175216

Abstract
Pulsed cathodic arc and pulsed magnetron sputtered WO_3 thin films were investigated using electron microscopy. It was found that the cathodic arc deposited material consisted of the α-WO_3 phase with a high degree of crystallinity. In contrast, the magnetron sputtered material was highly disordered making it difficult to determine its phase. Electron energy-loss spectroscopy was used to study the oxygen K edge of the films and it was found that the near-edge fine structures of films produced by the two deposition methods differed. The oxygen K-edge near-edge structures for various phases of WO_3 were calculated using two different self-consistent methods. Each phase was found to exhibit a unique oxygen K edge, which would allow different phases of WO_3 to be identified using x-ray absorption spectroscopy or electron energy-loss spectroscopy. Both calculation methods predicted an oxygen K edge for the γ-WO_3 phase which compared well to previous x-ray absorption spectra. In addition, a close match was found between the oxygen K edges obtained experimentally from the cathodic arc deposited material and that calculated for the α-WO_3 phase.

1. Introduction

Tungsten trioxide (WO_3) is an important transparent conducting oxide which exhibits interesting chromogenic properties allowing the material to reversibly change its optical state. This property is being investigated for 'smart windows', electro-optical components and display applications [1–3]. It can be deposited using several methods including sputtering [1, 2], evaporation [4, 5], pulsed laser deposition [6] and cathodic arc deposition [7]. In general, the microstructure and performance of the films depends on the method, deposition temperature and other process conditions, with mainly amorphous and structures reported [8]. Crystalline WO_3 is known to have a perovskite-type structure which undergoes up to 4 phase changes depending on the temperature [9]. Starting with a monoclinic (ε) phase at low temperatures [10], the structure transforms into either a triclinic (δ) [11, 9] or a different monoclinic phase (γ) [11, 9] at room temperature. At higher temperatures, orthorhombic (β) [12] and tetragonal (α) [13] phases occur at 480 °C and 770 °C, respectively. Although all phases are based on distorted WO_6 octahedra, each structure is subtly different and these differences could influence the electronic and other properties.

In this paper we investigate the microstructure of WO_3 thin films prepared using two different techniques: pulsed magnetron sputtering and pulsed cathodic arc deposition.

The differences between these two techniques are significant. Cathodic arc deposited films are formed from energetic and multiply charged ions [14–16] while films formed from a sputtered process are primarily from low energy neutrals [17], though energetic negative ions may be present [18]. The incident energy of the depositing particles is known to have an important influence on the microstructure [19, 20].

We employ transmission electron microscopy (TEM) and electron energy-loss spectroscopy (EELS) to characterize the films. Superimposed on each EELS absorption edge is structure (known as energy loss near-edge structure or ELNES) which arises because the final state wavefunction of the excited electron is modified by chemical bonding. This fine structure is identical to, and has its origin in the same process as the x-ray absorption near-edge structure (XANES). Therefore, the oxygen K-edge measured using either ELNES or XANES may provide a convenient way of distinguishing between the various phases of WO_3. However, the interpretation of near-edge structure is not straight forward and accurate theoretical modelling is essential [21]. We therefore employ the FEFF8.2 code, a real-space multiple scattering code, to calculate the oxygen K-edge of several possible WO_3 structures to compare with experiment. To validate our calculations, we compare the results to band structure calculations performed using WIEN2k and to previous x-ray absorption spectra [22].

2. Experimental details

Films of WO_3 were prepared by pulsed magnetron sputtering and pulsed cathodic arc deposition. For the magnetron deposition experiments, the chamber was initially pumped down to a base pressure of about 1.3×10^{-6} Torr (1.7×10^{-4} Pa) using a cryogenic pump with a pumping speed of 1500 l s^{-1}. The pumping speed was reduced using an adjustable gate valve to obtain a relatively high total pressure of 42 mTorr (5.6 Pa) with Ar and O_2 gas flows of 50 and 40 sccm, respectively. The gas was introduced into a gas plasma source of the constricted plasma source type [23] operated with a Pinnacle Plus power supply at 1500 W (pulsed-DC, 100 kHz, 1 μs reverse time). It was noted that the total pressure was reduced to about 36 mTorr (4.8 Pa) during deposition, which is due to the consumption of oxygen by the growing film. A 3 inch (76 mm) diameter W target with a sputter power of 1200 W was used. The substrate was placed 90 mm away from the sputtering gun and the plasma source. Total deposition time was 10 min.

For the pulsed cathodic arc deposition experiment, the chamber was pumped down to a base pressure of about 7×10^{-6} Torr (9×10^{-4} Pa) and backfilled with O_2 at a flow rate of 10 sccm to a pressure of about 6.6 mTorr (0.88 Pa). The pulsed arc source [24], equipped with a tungsten rod cathode and a 90° open-coil macroparticle filter, was fed from a switched capacitor bank (0.3 F) charged to 270 V, resulting in an arc current of about 180 A, limited by a 1.5 Ω resistor in series. The arc repetition rate was 3 pulses per second, with an arc duration of 3 ms. After 7600 pulses, a film thickness of 200 nm was obtained, with the holder placed about 90 mm from the filter exit. Throughout the deposition process, the sample holder was pulsed-biased to −200 V with a pulse cycle of 10 μs on (−200 V) and 90 μs off (ground).

The stoichiometry of the films were measured using x-ray photoelectron spectroscopy (XPS) performed on a VG Microlab 310F with a dual Al/Mg anode unmonochromated x-ray source operated at a power of 300 W and 15 kV excitation voltage. The sample was tilted such that the electron analyser normal to the sample surface collected the escaping electrons. Cross-section TEM specimens of the samples were prepared using mechanical polishing and ion beam thinning. These specimens were then analysed in a JEOL2010 TEM operating at 200 kV. To measure the ELNES, EELS spectra of the coatings were collected using a Gatan Imaging Filter operating in spectroscopy mode. The energy resolution was 1.8 eV as measured by the FWHM of the zero loss peak. All spectra were collected in imaging mode with a spectrometer entrance aperture of 2 mm.

3. Theoretical details

The oxygen K-edge for several possible WO_3 phases was calculated using the FEFF8.2 code [25] (which will be referred to as FEFF8 throughout this paper). FEFF8 is a real-space multiple scattering code which employs accurate self-consistent-field potentials to calculate the edge structure. Other features in the code include an energy dependent exchange correlation potential, the ability to use screened core-holes and Debye–Waller factors to treat the effects of vibrations. Full multiple scattering was used to calculate the oxygen K-edge for several WO_3 phases using the parameters in table 1. For all calculations, a core-hole and a muffin-tin overlap of 15% were used. The exchange potential was of the Hedin–Lundqvist type which is recommended for solids. Each of the WO_3 structures listed in table 1 has at least 2 unique oxygen positions. Therefore, the near-edge structure of each unique oxygen atom was modelled separately and then combined to provide an average.

Calculations of the oxygen K-edges were also performed using the WIEN2k code [26] on the tetragonal α-WO_3 phase and the monoclinic γ-WO_3 phase. The electron wavefunctions and eigenvalues are calculated by the full-potential (linearized) augmented plane-wave ((L)APW) + local orbitals (lo) method. Exchange and correlation were treated using the generalized gradient approximation (GGA). The parameter determining the size of the basis set, $R_{MT}K_{MAX}$, was set to 7. The muffin tin radii were chosen as large as possible but without overlapping spheres. The number of k-points in the irreducible Brillouin zone (BZ) was 90 for α-WO_3 and 54 for γ-WO_3. Convergence tests showed that this number of k-points were adequate. A core-hole was not included in the results presented here, as it only changed in the relative intensity of the peaks by a small amount, but with a considerable increase in computational time. The oxygen K-edge was calculated using the XSPEC subroutine within WIEN2k. Spectra were calculated for all inequivalent positions in the unit cell and an appropriate average taken. Differences between the different atomic sites were very small. Lorentzian broadening of 1.3 eV was included to account for the experimental energy resolution.

Table 1. Details of the crystallography of the phases used in the FEFF8 and WIEN2k calculations. The cluster size and full multiple scattering radius used in the FEFF8 calculations are also shown.

Structure	Symmetry	Space group	Lattice parameters	Cluster size	Calculation radius (Å)
α-WO_3 [13]	Tetragonal	$P4/nmm$	$a_o = 5.3031$ Å $c_o = 3.9348$ Å	161 atoms	6
β-WO_3 [12]	Orthorhombic	$Pmnb$	$a_o = 7.341$ Å $b_o = 7.570$ Å $c_o = 7.754$ Å	179 atoms	6
γ-WO_3 [11]	Monoclinic	$P2_1/n$	$a_o = 7.300\,84$ Å $b_o = 7.538\,89$ Å $c_o = 7.689\,62$ Å $\alpha = \gamma = 90°$ $\beta = 90.892°$	165 atoms	6
δ-WO_3 [11]	Triclinic	$P\bar{1}$	$a_o = 7.312\,78$ Å $b_o = 7.525\,40$ Å $c_o = 7.689\,54$ Å $\alpha = 88.847°$ $\beta = 90.912°$ $\gamma = 90.940°$	172 atoms	6
ε-WO_3 [10]	Monoclinic	Pc	$a_o = 5.277\,10$ Å $b_o = 5.155\,41$ Å $c_o = 7.662\,97$ Å $\beta = 91.975\,92°$	167 atoms	6.96

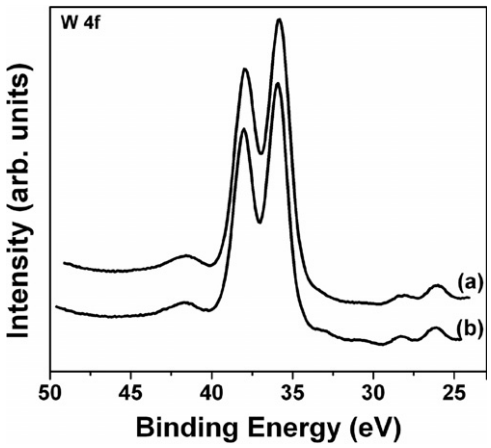

Figure 1. XPS spectra showing the W 4f peaks from the (a) cathodic arc and (b) magnetron sputtered films.

4. Results and discussion

XPS was performed on the films in the regions of the tungsten 4f and oxygen 1s binding energy peaks. Figure 1 shows the W 4f spectra for the (a) cathodic arc and (b) magnetron sputtered films. The peak positions were found to occur at 35.8 and 37.9 eV, consistent with previously reported peak positions for WO_3 [27]. The stoichiometry of the sputtered and cathodic arc deposited films was determined using peak area analysis to be $WO_{2.87}$ and $WO_{2.73}$, respectively. Therefore, both films are close to stoichiometric.

The corresponding cross-sectional TEM images of these samples are shown in figures 2(a) and (b). These images show the glass substrate on the left and the film running down the middle of the image. The microstructure of the sputtered film appeared highly disordered and this was confirmed by the selected area diffraction pattern shown in figure 3(a). It was not possible to index this diffraction pattern unambiguously to any particular phase. The cathodic arc deposited film was highly ordered and within the film large crystallites were found. The inset in figure 2(b) is a high resolution image of one of these crystals which reveals a crystal lattice. The selected area diffraction pattern from this crystalline region of this film is shown in figure 3(b). The pattern has been indexed to the α-WO_3 phase. This is an interesting result since a previous investigation of tungsten oxide films prepared using magnetron sputtering has exhibited an amorphous WO_3 structure [8]. The energetic plasma associated with cathodic arc deposition clearly had an impact on the microstructure on the resulting WO_3 producing the high temperature α-phase and improved crystallinity.

In figure 4 we compare the oxygen K-edges obtained using EELS from the magnetron sputtered and the cathodic arc deposited coatings. Note that the main features have been labelled for clarity and due to experimental errors in the energy offset, peak A has been aligned to 530.7 eV as measured previously using x-ray absorption spectroscopy for a γ-WO_3 powder standard [8]. The features in the oxygen K-edge of the magnetron sputtered sample are broad, probably the result of the high level of disorder in this sample. In contrast, the fine structure in the cathodic arc sample is more distinct and shows an additional peak at 551.7 eV (labelled 'G' in the figure).

The oxygen local s and p projected density of states (DOS) calculated using FEFF8 for the α and γ phases are shown in figure 5. Differences in the DOS are clearly seen between these phases, particularly in the pDOS above the Fermi energy which is expected to be reflected in the near-edge structure of the corresponding oxygen K-edge. Figure 6 shows a comparison of the oxygen K-edges for each phase of WO_3 calculated using FEFF8 with 0.5 eV of broadening added to the calculation. In order to compare with the experiment, peak A has been aligned

Table 2. The position (eV) of the main features in the experimental and calculated oxygen K-edges. Note that the experimental and calculated values have been shifted so that peak A aligns with previous x-ray absorption spectroscopy measurements of a powder standard γ-WO_3.

Sample/phase	A	B	C	D	E	F	G	H
Magnetron sputtered	530.7	—	535.5		541.8		—	563.4
Cathodic arc	530.7	—	537.5		543.1		551.7	568.3
am-WO_3 [8]	530.5	532.0	536.4		542.5		—	565.0
γ-WO_3 [8]	530.7	531.7	535.4	537.6	541.1	543.8	556.1	567.2
α-FEFF8	530.7	535	537.9	540.3	545.3	548.2	555.8	571.3
β-FEFF8	530.7	535.9	538.1	540.9	545.6	548.7	556.2	573.2
γ-FEFF8	530.7	—	537.6	541	544.3	549.9	558.7	572.3
δ-FEFF8	530.7	—	538.6	542	545.7	548.4	559.6	572.8
ε-FEFF8	530.7	—	537.5	541.7	544.3	548.6	558.8	572.2
α-WIEN2k	530.7	—	537.7		543		552.7	567.8
γ-WIEN2k	530.7	—	536.8		542.9		554.8	566.7

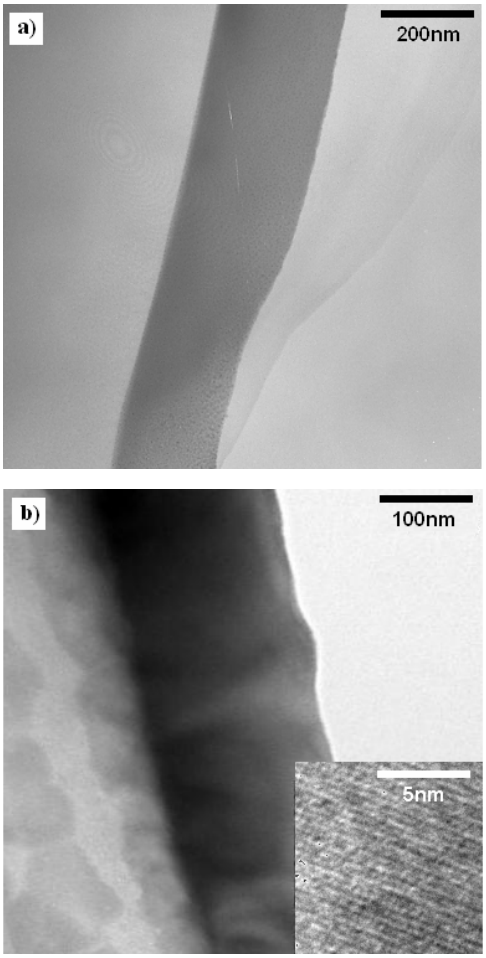

Figure 2. Cross-sectional TEM Images of the deposited films. (a) Magnetron sputtered sample, (b) cathodic arc sample. Inset: high resolution image of cathodic arc sample.

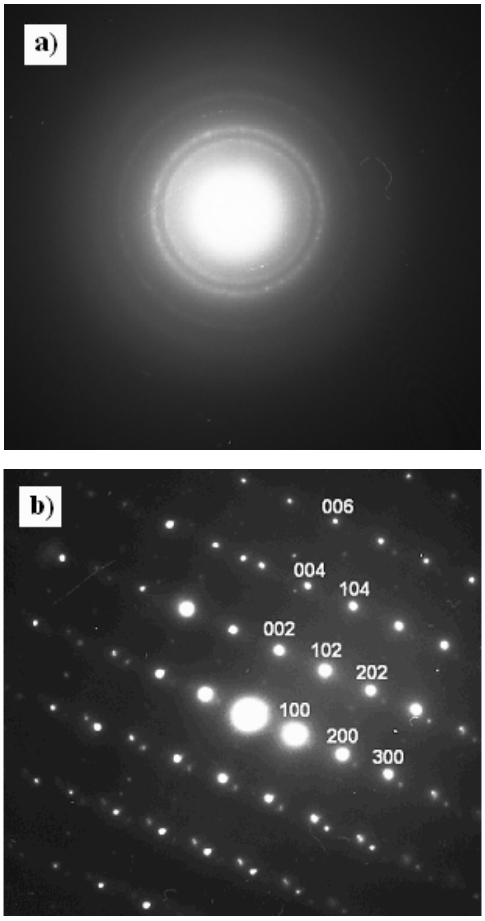

Figure 3. Selected area diffraction patterns of the (a) magnetron sputtered and (b) cathodic arc films shown in figure 2. The diffraction pattern in (b) has been indexed to γ-WO_3.

to 530.7 eV as measured previously for γ-WO_3 [8]. Clearly, each phase has a unique near-edge structure despite the fact that each phase has a similar atomic arrangement based on WO_6 octahedra. It has been suggested [8] that peak G intensity is dependant on the W–O–W bond angle which is determined by the lattice parameters, in particular the angle between axes. We also find that the intensity of this peak is related to the W–O–W bond angle, and is strongest in structures with orthogonal bonds. This can be seen in figure 6, whereby the two phases which have a 90° bond angle show the strongest G peak. The 'H' peak is attributed to single scattering processes from the nearest neighbour oxygen atoms [8].

Table 2 lists the energies of the main features (labelled in figure 6) found in the FEFF8 calculations, along with the peak positions determined using EELS (labelled in figure 4) and results reported elsewhere [8]. Generally, the energies of the features do not vary significantly between the phases, although

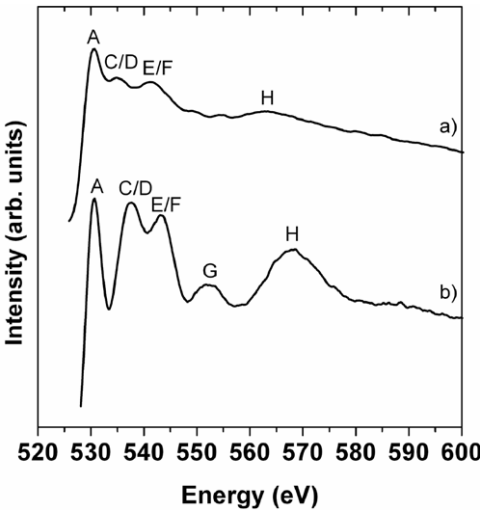

Figure 4. Oxygen K-edge EELS spectra for the two experimental samples. (a) Magnetron sputtering, (b) cathodic arc. The main features have been labelled for clarity.

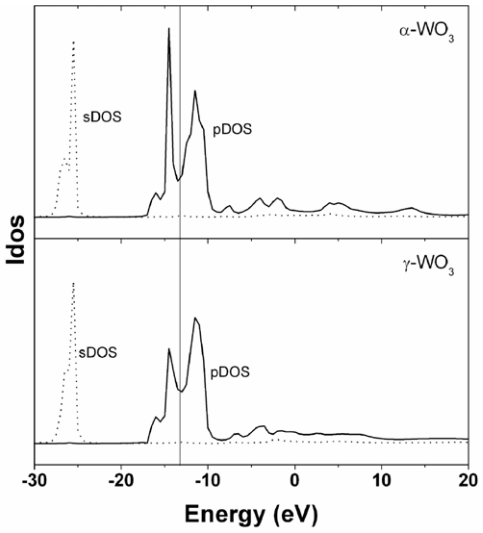

Figure 5. The local s and p projected density of states for oxygen calculated using FEFF8 for the α and γ phases of WO_3. The vertical line indicates the position of the Fermi energy.

the relative intensities do. Table 2 also shows the positions of features which could be resolved from the experimental work shown in figure 4. Due to experimental broadening, particularly in the EELS measurements, some adjacent features are not resolved and appear as a single peak. A similar broadening of features was observed in previously reported x-ray absorption results from magnetron sputtered amorphous WO_3 films [8].

Figure 7(a) compares the oxygen K-edge of γ-WO_3 calculated using FEFF8 and that obtained using WIEN2k. Also shown is the oxygen K-edge obtained using XANES for the γ-WO_3 powder standard [8]. Overall, the results are similar with the main features reproduced using both methods. The FEFF8 calculation does include the doublet (features E and F) at approximately 540 eV which is not reproduced in WIEN2k calculation.

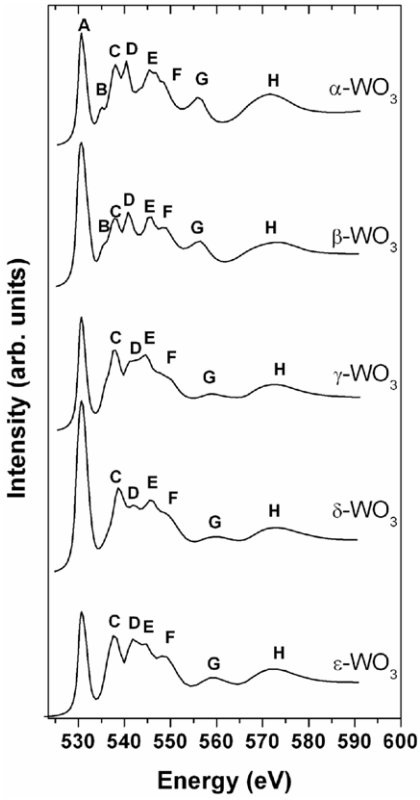

Figure 6. The calculated oxygen K-edge near-edge structures for the known phases of WO_3. The main features have been labelled and their energies have been listed in table 2.

Figure 7(b) compares the EELS spectrum from the cathodic arc deposited sample with that calculated using FEFF8 and WIEN2k for α-WO_3. There is a good agreement between theory and experiment. As with the case of γ-WO_3, WIEN2k does not reproduce the relative intensities of peaks C/D and E/F, while the peak positions of the peaks B to H calculated using FEFF8 are shifted upwards by approximately 3–4 eV away from the experimental values (see table 2). The discrepancy in the positions may be the result of errors in the calculation of the potential in the FEFF8 code, the accuracy of which is critical for reproducing the position of features close to the threshold [28]. It was found that reducing the size of the muffin tin potentials effectively 'shrinks' the graph along the energy scale, resulting in a better fit. Also shown in figure 7(b) (thin line) is the FEFF8 calculation using a muffin tin radius, where the muffin tins were set to have a 10% separation. The overall fit, including both peak positions and intensity, is improved.

The real-space approach employed in FEFF8 allows us to explore the variation in the near-edge structure as a function of cluster size around the absorbing atom. Figure 8 shows the variation in the oxygen K-edge as the cluster size increases. The basic edge shape is formed for a small cluster consisting of an oxygen atom bonded to its two adjacent tungsten atoms. The dominant first peak A appears when the absorbing oxygen atom is surrounded by its eight nearest oxygen atoms, four from each adjoining octahedral unit. The next significant change in the oxygen K-edges occurs for a cluster size of

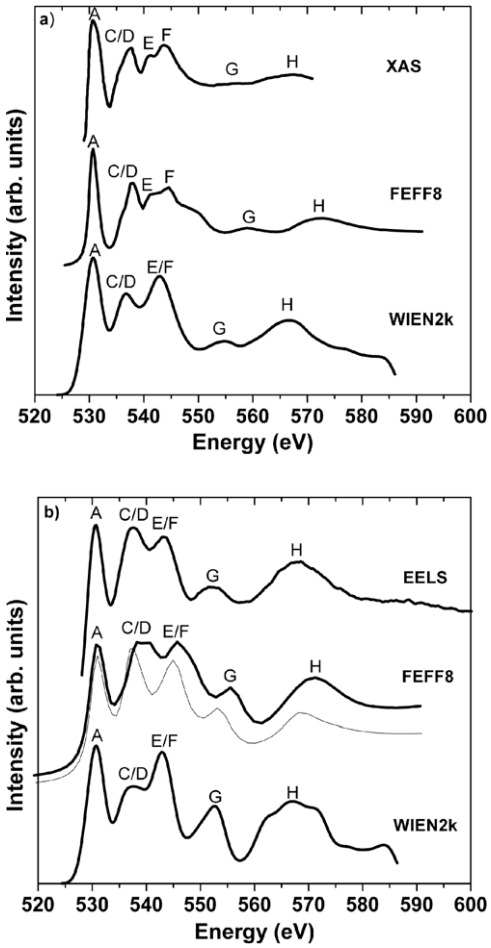

Figure 7. Comparison of the oxygen K-edge of calculated using FEFF8 and WIEN2k. These are compared to (a) γ-WO_3 obtained using x-ray absorption spectroscopy [8] and (b) α-WO_3 obtained using EELS. Note that the thin line overlaying the FEFF8 calculations in (b) was performed using a different muffin tin overlap (see text).

twelve atoms, when the two adjoining octahedral units are completed and peaks C/D and E/F form.

5. Conclusions

The structure of tungsten trioxide thin films was found to depend on the fabrication method. The energetic ions associated with cathodic arc deposition produced a film with a well-ordered tetragonal structure. On the other hand, magnetron sputtering produced a highly disordered material which, due to the limited energy resolution of EELS, was difficult to assign to a particular phase. It was shown that the FEFF8 code is able to distinguish subtle differences in the oxygen K-edge for various phases of WO_3. The calculated oxygen K-edge using both FEFF8 and WIEN2k for the γ-WO_3 phase was found to match well with previous published experimental x-ray absorption results. There was also a good match between the calculated oxygen K-edge for the α-WO_3 phase and that found using EELS for the cathodic deposited film. Finally, we have shown that the near-edge structure on the oxygen K-edge can be used to identify the phase of WO_3.

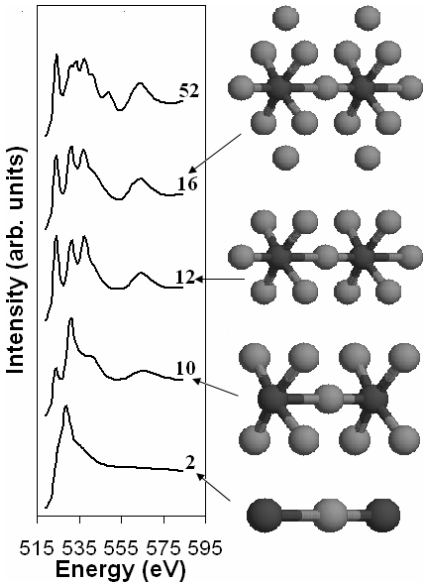

Figure 8. Calculated oxygen K-edge's for the α-WO_3 phase for various numbers of atoms surrounding the absorbing oxygen (left). A graphical representation of the clusters is also shown (right), with light atoms and dark atoms representing oxygen and tungsten atoms respectively.

Acknowledgments

The authors acknowledge the financial assistance provided by the Australian Research Council (ARC). A/Professor Johan du Plessis is thanked for his assistance with the XPS analysis. S Lim would like to acknowledge the American Australian Association for the 2004 ANZ fellowship.

References

[1] Cui H N, Costa M F, Teixeira V, Porqueras I and Bertran E 2003 *Surf. Sci.* **532–535** 1127–31
[2] Akl A A, Kamal H and Abdel-Hady K 2003 *Physica* B **325** 65–75
[3] Granquist C G 1995 *Handbook of Inorganic Electrochromic Materials* (Amsterdam: Elsevier)
[4] Gillet M, Al-Mohammad A and Lemire C 2002 *Thin Solid Films* **410** 194–9
[5] Shigesato Y, Murayama A, Kamimori T and Matsuhiro K 1988 *Appl. Surf. Sci.* **33/34** 804–11
[6] Rougier A, Portemer F, Quede A and El Marssi M 1999 *Appl. Surf. Sci.* **153** 1–9
[7] Tay B K, Zhao Z W and Chua D H C 2006 *Mater. Sci. Eng.* R **52** 1–48
[8] Purans J, Kuzmin A, Parent P and Laffon C 2001 *Electrochim. Acta* **46** 1973–6
[9] Aird A, Domeneghetti M C, Mazzi F, Tazzoli V and Salje E K H 1998 *J. Phys.: Condens. Matter* **10** L569–74
[10] Salje E K H, Rehmann S, Pobell F, Morris D, Knight K S, Herrmannsdorfer T and Dove M T 1997 *J. Phys.: Condens. Matter* **9** 6563–77
[11] Woodward P M, Sleight A W and Vogt T 1995 *J. Phys. Chem. Solids* **56** 1305–15
[12] Salje E 1977 *Acta Crystallogr.* B **33** 574–7
[13] Locherer K R, Swainson I P and Salje E K H 1999 *J. Phys.: Condens. Matter* **11** 4143–56
[14] Anders A 1997 *Phys. Rev.* E **55** 969–81

[15] Oks E M, Anders A and Brown I G 1996 *IEEE Trans. Plasma Sci.* **24** 1174–83
[16] Anders A and Yushkov G Y 2002 *J. Appl. Phys.* **91** 4824–32
[17] Mattox D M 1998 *Handbook of Physical Vapor Deposition (PVD) Processing* (Westwood, NJ: Noyes Publications)
[18] Mráz S and Schneider J M 2006 *Appl. Phys. Lett.* **89** 051502
[19] Bilek M M M, Tarrant R N, McKenzie D R, Lim S H N and McCulloch D G 2002 *IEEE Trans. Plasma Sci.* **31** 939–44
[20] Brown I G 1998 *Annu. Rev. Mater. Sci.* **28** 243–69
[21] Keast V J, Scott A J, Brydson R, Williams D B and Bruley J 2001 *J. Microsc.* **203** 135–75
[22] Schwarz K, Blaha P and Madsen G K H 2002 *Comput. Phys. Commun.* **147** 71–6
[23] Anders A and Yushkov G Y 2007 *Rev. Sci. Instrum.* **78** 043304–7
[24] MacGill R A, Dickinson M R, Anders A, Monteiro O R and Brown I G 1998 Streaming metal plasma generation by vacuum arc plasma guns *Proc. 7th Int. Conf. on Ion Sources* (Shirahama: AIP) pp 801–3
[25] Ankudinov A L, Ravel B, Rehr J J and Conradson S D 1998 *Phys. Rev.* B **58** 7565
[26] Hebert C 2007 *Micron* **38** 12–28
[27] *Auger and Xray Photoelectron Spectroscopy* 1990 vol 1 (New York: Wiley)
[28] Modrow H, Bucher S, Rehr J J and Ankudinov A L 2003 *Phys. Rev.* B **67** 035123